JOURNAL OF VIROLOGY, May 2002, p. 4456–4466 Vol. 76, No. 9
0022-538X/02/$04.00+0 DOI: 10.1128/JVI.76.9.4456–4466.2002

New Insights into the Spring-Loaded Conformational Change of Influenza Virus Hemagglutinin†

Jennifer A. Gruenke,[1] R. Todd Armstrong,[1] William W. Newcomb,[2] Jay C. Brown,[2] and Judith M. White[1,2]*

Department of Cell Biology[1] and Department of Microbiology,[2] University of Virginia, Charlottesville, Virginia 22908

Received 29 October 2001/Accepted 21 January 2002

Influenza virus hemagglutinin undergoes a conformational change in which a loop-to-helix "spring-loaded" conformational change forms a coiled coil that positions the fusion peptide for interaction with the target bilayer. Previous work has shown that two proline mutations designed to disrupt this change disrupt fusion but did not determine the basis for the fusion defect. In this work, we made six additional mutants with single proline substitutions in the region that undergoes the spring-loaded conformational change and two additional mutants with double proline substitutions in this region. All double mutants were fusion inactive. We analyzed one double mutant, F63P/F70P, as an example. We observed that F63P/F70P undergoes key low-pH-induced conformational changes and binds tightly to target membranes. However, limited proteolysis and electron microscopy observations showed that the mutant forms a coiled coil that is only ~50% the length of the wild type, suggesting that it is splayed in its N-terminal half. This work further supports the hypothesis that the spring-loaded conformational change is necessary for fusion. Our data also indicate that the spring-loaded conformational change has another role beyond presenting the fusion peptide to the target membrane.

Hemagglutinin (HA) is a glycoprotein of influenza virus which mediates fusion of the viral and host membranes. HA binds the virus to a target cell, allowing the virus to be endocytosed. The low-pH environment of the endosome then triggers conformational changes in HA, which cause fusion. The viral genome enters the cytoplasm, and infection proceeds. HA is the most extensively studied viral fusion protein and therefore serves as a paradigm for enveloped virus fusion.

Following synthesis and trimerization, each member of the HA homotrimer is cleaved to two subunits, HA1, containing the sialic acid binding site, and HA2, containing the N-terminal fusion peptide and the C-terminal transmembrane domain. Cleavage primes HA for transition from the native, metastable state to the final, lowest-energy state upon acidification (8). The structures of HA in the native form and a fragment of the low-pH form have been solved by X-ray crystallography (Fig. 1) (6, 9, 31). In the native state, HA2 trimerizes through the formation of a parallel coiled coil. At the N terminus of the native coiled coil (Fig. 1A, yellow), a loop region (HA2 55-75) (Fig. 1A, dark blue; designated B region in reference 6) connects to a second α-helix (Fig. 1A, green), which runs antiparallel to the first. At the N terminus of the second α-helix is the fusion peptide (Fig. 1A, red), which is buried in the center of the native trimer. The three HA1 subunits (Fig. 1A, gray) cover the HA2 subunits, making trimeric contacts and acting as a clamp. In the fragment of low-pH-treated HA, in which the fusion peptide, transmembrane domain, and most of HA1 have been removed, the structure of HA2 is quite different (Fig. 1B). The B loop region (dark blue) has refolded into an α-helix, connecting the two original helices of the HA2 ectodomain into one coiled coil, with the fusion peptide (red) at its extreme N terminus. This conformational change is referred to as the spring-loaded conformational change (7). Dramatic changes also occur at the C-terminal end of the original coiled coil. A region of six amino acids has unfolded to a loop (purple), and the helix C-terminal to the new loop has flipped to lie antiparallel to the coiled coil (orange). The crystal structure of a recombinant, slightly longer form of HA2 (Fig. 1B) shows that the region between the end of this helical hairpin structure and the transmembrane domain forms an extended chain that lies in the groove between helices of the N-terminal parallel coiled coil (Fig. 1B, light blue). Hence, in the final low-pH state (Fig. 1B), the transmembrane domain lies near the fusion peptide (9).

The differences in structure between the native and low-pH forms of HA suggest a mechanism for fusion in which the head groups (Fig. 1A, gray) separate and then the spring-loaded conformational change occurs, moving the fusion peptides toward the target membrane. The fusion peptides embed in the target membrane, and the helix-to-loop conformational change then pulls the fusion peptide, and therefore the attached target membrane, toward the transmembrane domain (14, 29; see also the White laboratory website). Similar models have been advanced for other viral and cellular fusion proteins that contain coiled coils. Several sets of data have, however, been used to argue against the importance of the spring-loaded conformational change. First, head group separation was not detected when low pH was applied at low temperatures (0°C), even though fusion could occur under these conditions (26). Furthermore, fusion at higher temperatures was shown to occur before head group separation was detected by electron microscopy (EM) (25). Because it seems apparent that some

* Corresponding author. Mailing address: Dept. of Cell Biology, UVA Health System, School of Medicine, P.O. Box 800732, Charlottesville, VA 22908. Phone: (434) 924-2593. Fax: (434) 982-3912. E-mail: jw7g@virginia.edu.

† This paper is dedicated to the memory of Don Wiley.

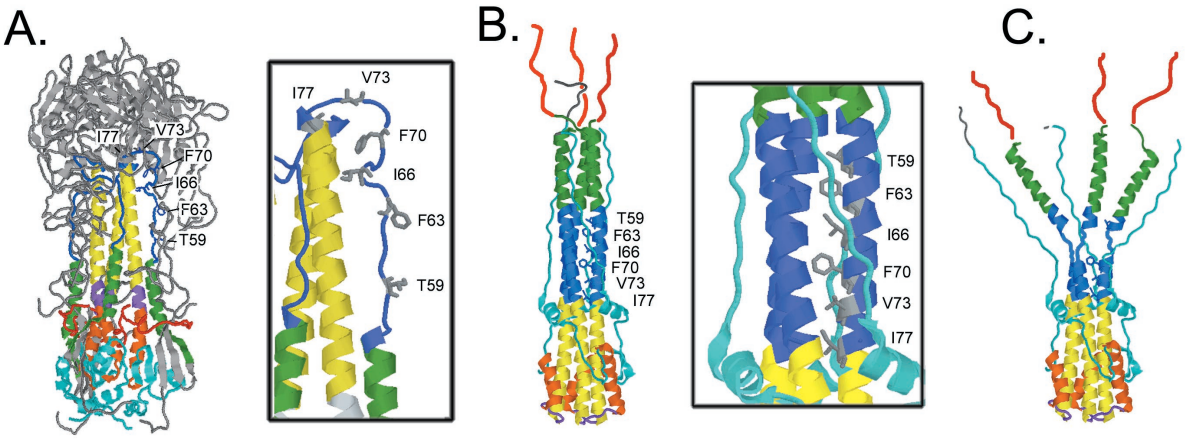

FIG. 1. Location of mutants and model of disrupted coiled coil. (A) Structure of the native HA ectodomain (31) (Protein Data Base [PDB] accession no. 2HMG). A detail of the relevant region of HA2 is boxed. (B) Structure of *E. coli*-produced HA2 (EHA2) (9) (PDB accession no. 1QU1). Residues replaced by proline in this study are indicated. The boxed figure shows detail. (C) Proposed model of an HA coiled coil that is disrupted by proline substitutions. The disrupted region shown is that predicted for F63P/F70P HA and would vary in position for different mutants. The angle of splayed helices is not intended to be absolute; rather the disrupted region is predicted to be somewhat flexible. For all, HA1 is gray and HA2 is colored. Fusion peptides (red) in panels B and C have been drawn in. For all, the A region is green, the B region is dark blue, the C region is yellow, the kink (helix-to-loop) region is purple, the D region is orange, and the region C terminal of the D region is light blue.

head group separation is required for complete coiled-coil formation, it was argued that fusion occurs prior to the spring-loaded conformational change. These and other lines of evidence led to alternate models for HA fusion which do not require the spring-loaded conformational change (3, 5, 26) (see Discussion).

We previously showed that a mutant containing proline at residue 55 of the B loop was impaired for fusion, and mutant V55P/S71P, with two B-loop mutations, displayed no fusion (21). Although these findings supported the importance of the spring-loaded conformational change, our prior study did not directly address coiled-coil formation and did not analyze critical conformational changes in HA2. Hence, the root cause for the fusion defects was not uncovered. Because of these limitations and because the role of the spring-loaded conformational change remains controversial (see Discussion), we further explored its function. We first substituted prolines for all of the residues in the B loop that are found at "a" and "d" positions in the final coiled coil; we also made two new double proline substitutions in this region. We asked the following three questions. Are any of the proline-substituted mutants impaired for fusion? If so, at what stage does this occur (i.e., critical conformational changes or target membrane interactions)? Do fusion-impaired mutants form complete coiled coils? None of the double mutants caused any fusion. Double mutant F63P/F70P was analyzed in detail. Like wild-type (WT) HA, F63P/F70P underwent key conformational changes, including head group separation and fusion peptide exposure, and bound tightly to target membranes. Several lines of evidence indicated, however, that, instead of forming a complete coiled coil, F63P/F70P formed a coiled coil that was only about one-half the length of that formed by the WT and that was splayed in its N-terminal half. Our results demonstrate that complete coiled-coil formation is not necessary for fusion peptide exposure and membrane binding but is crucial for fusion to progress from target membrane binding to membrane merger.

MATERIALS AND METHODS

Antibodies. A rabbit polyclonal antibody to SHA2 was generated by Covance Laboratories (Vienna, Va.). The rabbit polyclonal CHA1 antibody and mouse monoclonal antibody (MAb) 12CA5 were as previously described (1, 30). Mouse MAb LC89 was a gift from J. Skehel (National Institute for Medical Research, London, United Kingdom). The anti-fusion peptide rabbit polyclonal antibody, directed against the fusion peptide sequence of Japan HA, was a gift from L. Chernomordik (National Institutes of Health [NIH], Bethesda, Md.).

Mutagenesis. Mutants were generated from X:31 HA with the QuickChange site-directed mutagenesis kit (Stratagene). Approximately 300-bp segments of all mutant cDNAs were sequenced to determine the presence of the desired, and the absence of extraneous, mutations. F63P/F70P and I66P/V73P were sequenced in full.

Expression of WT and mutant HAs. HAs were expressed in CV-1 or NIH 3T3 cells by using the vaccinia virus T7 system as described previously (1). For some transfections we used liposomes made of a 2:1 (mol/mol) ratio of PE (L-[a]-phospatidylethanolamine, dioleoyl [C18:1, cis-9]; Sigma Chemical Company)/DDAB (dimethyldioctadecyl-ammonium bromide; Sigma) and extruded through a 0.05-μm-pore-size membrane (Whatman Nuclepore) instead of the Mirus Transit reagent. For these transfections, 0.4 ml of Opti-MEM (Gibco) per 6-cm-diameter dish of cells was mixed with 1 to 5 μg of plasmid DNA, 2 μg of protamine sulfate (Sigma) (33), and liposomes (70 μg/ml, final concentration), incubated for 30 min at room temperature (RT), and then added to 1.5 ml of Opti-MEM on infected cells. Expression levels for the two transfection methods were comparable. Cells were harvested 18 to 24 h after transfection.

Cell lysis and release of GPI-HA. Cells expressing full-length HA were lysed in phosphate-buffered saline (PBS) containing 1% NP-40 and protease inhibitors as described previously (12). Cells expressing glycosylphosphatidylinositol-linked HA (GPI-HA) were removed from the plate in PBS plus 0.5 mM (each) EDTA and EGTA, pelleted in a microcentrifuge, resuspended in 40 μl of PBS containing protease inhibitors and 5 μl of crude phosphatidylinositol phospholipase C (PIPLC) preparation (prepared as described in reference 16)/plate, and incubated at 37°C for 1 h to release the GPI-HA. Cells were pelleted, and the supernatant containing the released GPI-HA was collected.

Purification of PIPLC-released GPI-HA. CV-1 cells were transfected and treated with trypsin and PIPLC as described above. Supernatants from PIPLC digestions were treated with neuraminidase (NA; 1 mg/ml for 15 min at RT), and then applied to 5 to 25% sucrose gradients, which were centrifuged in a TLS55

rotor at 200,000 × *g* for 4 h at 4°C. Fractions containing HA, detected using a spot blot analysis, were further purified on ricin-agarose essentially as described previously (21).

Immunoprecipitation and Western blot analysis. Cell lysates or PIPLC-released GPI-HA was mixed with a solution containing10 μl of protein A-agarose (Boehringer Mannheim), 1 to 2 μl of an antibody, and protease inhibitors. NP-40 (0.1%) was added to GPI-HA samples. Samples were incubated at 4°C for 2 h with constant mixing. Beads from lysate samples were washed serially with HSA (12.5 mM K_2HPO_4 [pH 7.4], 0.6 M NaCl, 0.02% NaN_3), PBSN (PBS, 0.1% NP-40), SA (12.5 mM K_2HPO_4 [pH 7.4], 0.3 M NaCl), and 20 mM Tris, pH 8.3. Beads from GPI-HA samples were washed three times with PBSN. Beads were suspended in sample buffer (Bio-Rad bulletin 9672) with 5% (vol/vol) β-mercaptoethanol, boiled, and separated by sodium dodecyl sulfate–12% polyacrylamide gel electrophoresis (SDS–12% PAGE). Proteins were transferred to nitrocellulose membranes (Schleicher & Schuell, Keene, N.H.), which were then blocked and probed as previously described (1)

Conformational-change assays. WT and mutant GPI-HAs were expressed in CV-1 cells, treated with trypsin to activate HA0, biotinylated, and released with PIPLC. The pH of the samples was adjusted using a predetermined amount of HCl for 2 min at 37°C, and then the samples were reneutralized with NaOH. Samples were then immunoprecipitated with conformation-specific antibodies or Site A, a non-conformation-specific antibody, separated by SDS-PAGE, transferred to nitrocellulose, and detected with horseradish peroxidase-conjugated streptavidin.

Liposome binding. To prepare liposomes, phosphatidylcholine (PC)-cholesterol (at a 2:1 molar ratio) dissolved in chloroform was dried under a stream of nitrogen gas, lyophilized overnight, suspended in PBS, and then extruded through a 0.1-μm-pore-size filter. PIPLC-released GPI-HA was mixed with liposomes, the pH was adjusted to 5.0 for 30 s at 37°C, and then samples were reneutralized. Samples were then analyzed on sucrose flotation gradients essentially as described previously (15). Where specified, urea at a final concentration of 6 M or KI at a final concentration of 1 M was added after reneutralization. Centrifugation was carried out in a TLA-100 at 197,000 × *g* for 90 min at 4°C. Gradient fractions were then analyzed for HA by SDS-PAGE and Western blotting with the CHA1 antibody.

RBC labeling and fusion. Human red blood cells (RBCs) were labeled with the lipid dye octadecylrhodamine (R18; Molecular Probes) and aqueous-content dye carboxyfluorescein (Molecular Probes) as previously described (18), and static fusion assays were performed as previously described (1). For examination of fusion kinetics, CV-1 cells grown on plastic coverslips were prepared and R18-labeled RBCs were bound as described above. Coverslips were assembled in a flow chamber (Warner Instrument Corp., Hamden, Conn.) on a temperature-controlled stage at 37°C. Fusion buffer prewarmed to 37°C was injected into the chamber, and images were collected at 20-s intervals. Fusion was quantitated using NIH Image software to integrate the intensity of fluorescence of a given number of RBCs (bound at a ratio of 1 to 3 RBCs/CV-1 cell) for each frame in the series of images.

NA-resistant RBC binding. NIH 3T3 cells were plated overnight in 3.5-cm-diameter polylysine-coated dishes and then transfected with WT HA or F63P/F70P HA as described above. After 24 h, cells were trypsin treated to activate HA0 and returned to the incubator for 2 h. The cells were then treated with 0.1 mg of NA (type V from *Clostridium perfringens*; Sigma) for 10 min at RT to optimize RBC binding. R18-labeled RBCs were bound to the cells, and cells were incubated at neutral or low pH (pH 4.9 for 15 min at RT). Cells were treated with 0.5 mg of NA/ml for 10 min at RT to detach adhered, but not fused, RBCs. The cells were then directly squirted with buffer to remove unfused RBCs. Cells were imaged with a fluorescence microscope as described above.

Rosette formation. Purified PIPLC-released GPI-HA was incubated at pH 5.0 or 7.2 for 10 min at RT, and then acidified samples were reneutralized. Samples were applied to 5 to 25% sucrose gradients, which were centrifuged in a TLS55 rotor for 4 h at 200,000 × *g* and 4°C. The gradients were fractionated and analyzed for HA with a spot blot (Mini-fold I; Schleicher & Schuell) and the CHA1 antibody.

EM. Purified PIPLC-released GPI-HA was mixed with liposomes (1:1 [mol/mol] ratio of PC to cholesterol) that had been extruded through an 0.05-μm-pore-size membrane. The mixture was acidified to pH 5.0 for 5 min at RT and then reneutralized. Samples were applied to Formvar and carbon-coated copper grids, stained with 1% sodium silicotungstate (pH 7.0), and examined with a Philips 400 T transmission electron microscope operated at 80 keV.

Purification of SHA2. Mutant F63P/F70P was constructed with an *Escherichia coli* expression vector containing the coding sequence for a fragment of HA2 (SHA2, residues 33 to 127 of X:31 strain; gift from Y. K. Shin, University of California). Plasmids were transformed into *E. coli* BL21(DE3), which was grown in Luria broth containing ampicillin (75 μg/ml), and induced with 0.5 mM IPTG (isopropyl-β-D-thiogalactopyranoside; Eppendorf, Westbury, N.Y.). The cells were harvested by centrifugation and then resuspended in 10 mM Na_2HPO_4, pH 7.0, containing protease inhibitors. The cell pellet was French pressed at 12,000 lb/in^2 two or three times. The crude cell extract was centrifuged to remove debris. The supernatant was applied to a DEAE-cellulose column (Sigma). The column containing WT SHA2 was washed with 150 mM NaCl, and then the protein was eluted with 600 mM NaCl. For F63P/F70P SHA2, the column was washed with 100 mM NaCl and then eluted with 150 mM NaCl. The peak fractions contained SHA2 were purified to greater than 95%.

CD. Purified SHA2 was concentrated and exchanged into 10 mM Na_2HPO_4, pH 7.0, with a Centricon (Millipore Corp., Bedford, Mass.; molecular weight cutoff, 10,000). Protein concentration, determined by bicinchoninic acid assay (Bio-Rad), was adjusted to 1.0 to 1.5 mg/ml. Circular dichroism (CD) measurements were taken with a J-720 spectropolarimeter (Jasco, Easton, Md.) and a 1-mm-path-length quartz cuvette. α-Helicity was calculated by using an average of three measurements of the CD signal at 222 nm. For samples scanned at pH 5.0, a predetermined amount of 1 M HCl was added immediately before the sample was scanned.

Thermolysin digestion of GPI-HA and SHA2. GPI-HA was released from transfected CV-1 cells as described above. Samples were either left at neutral pH or adjusted to pH 5. Thermolysin digestions were then carried out as described in the legend to Fig. 7. Reactions were quenched with EDTA, and samples were analyzed by SDS-PAGE and Western blotting (with the SHA2 antibody).

SHA2 cross-linking. WT or F63P/F70P SHA2 (300 ng) was incubated with the indicated concentration of BS3 (bis[sulfosuccinimidyl]suberate; Pierce) for 30 min at RT in 10 mM Na_2HPO_4, pH 7.0. Samples were then boiled in SDS-containing sample buffer, and proteins were separated by SDS–15% PAGE followed by Western blotting (1) with the SHA2 antibody.

Standard assays. Trypsin treatment of cells to cleave HA0 to HA1 and HA2 was performed as previously described (1), except that 5 μg of trypsin/ml was used, and trypsin was quenched with 1% fetal bovine serum. Cell surface proteins were biotinylated by incubation with 0.5 mg of sulfo-*N*-hydroxysuccinimide–LC–biotin (Pierce, Rockford, Ill.)/ml in PBS for 15 min at 37°C. Cells were washed three times with PBS to remove excess biotin. Sucrose gradient analysis of trimer formation was performed as described previously (21) except that PBS was used in place of MES (morpholineethanesulfonic acid)-saline, and centrifugation was done at 200,000 × *g* for 5 h at 4°C in a TLS55 rotor. Fluorescence-activated cell sorter (FACS) analysis and production of modified vaccinia virus Ankara were as previously described (1). HA crystal structures (Fig. 1, 9C, and 10C) were downloaded from the Protein Database, displayed in Rasmol (23), and modified with Adobe Photoshop. Figure 10C was made with the program Protein Explorer.

RESULTS

To explore whether the spring-loaded conformational change is necessary for fusion and, if so, for what aspect of fusion, we substituted proline at all "a" and "d" positions of the B loop region of HA (Fig. 1A and B). We also made two new double-proline substitutions. The mutants were tested for fusion activity (lipid mixing and content mixing) and for key conformational changes, including head group separation, fusion peptide exposure, the helix-to-loop transition, and hydrophobic attachment of HA to target membranes. We also analyzed the structures of several mutants for protease sensitivity and rosette formation, and by CD and EM.

Expression and processing. The new mutants are T59P, F63P, I66P, F70P, V73P, I77P, F63P/F70P, and I66P/V73P (Fig. 1A and B). All mutants were expressed at approximately the same level and, upon treatment with trypsin but not chymotrypsin, were cleaved (Fig. 2A). All mutants migrated to the same position of a sucrose gradient as WT HA, indicating that they all form trimers (Fig. 2B).

Fusion activity. After exposure to pH 5.0 for 10 min at RT, cells expressing all single-proline-substitution mutants, except T59P, showed an extent of fusion similar to that for the WT as judged by profiles of the diffusion of lipid and content fluores-

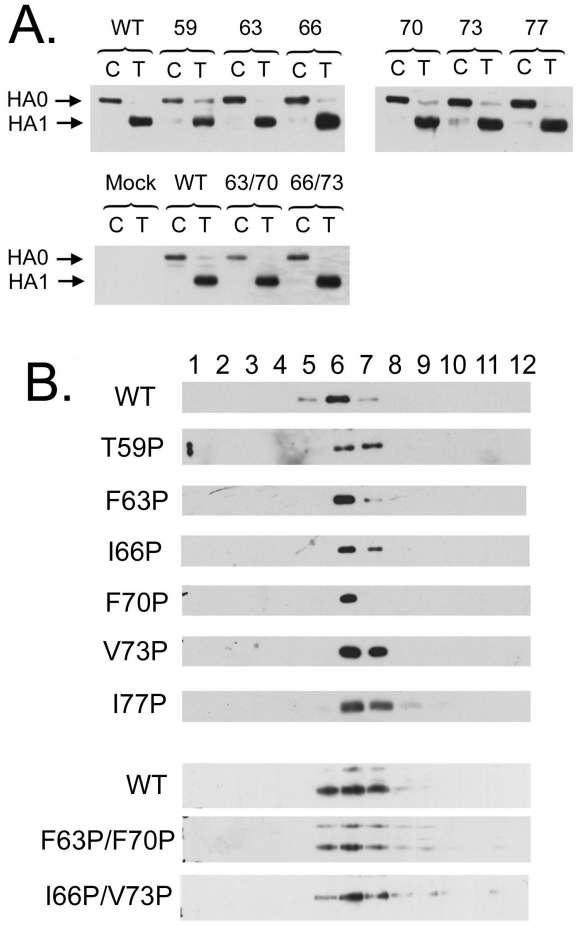

FIG. 2. Expression, trypsin cleavage, and trimer formation of mutant HAs. (A) CV-1 cells expressing WT or mutant HA were treated with trypsin (T) or chymotrypsin (C), separated by SDS–12% PAGE, and analyzed by Western blotting with the CHA1 antibody. (B) Lysates from trypsin-treated cells were run on sucrose gradients and analyzed by Western blotting with the CHA1 antibody. Fraction 1 is from the top of the gradient.

cent probes into cells (Fig. 3A and C). When cells expressing T59P were reacidified for an additional 10 min at 37°C, however, they showed a large amount of dye transfer (Fig. 3C).

We scrutinized the time course of fusion of the B loop mutants using video microscopy. T59P HA promotes fusion, but with a longer lag time than the WT and with a reduced rate and extent, similar to the previously described V55P HA (21) (Fig. 3B). Although the extent of fusion mediated by T59P HA was variable (compare Fig. 3B and C), in all experiments its lag time before fusion was increased and its rate of fusion was decreased. Cells transfected with either of double point mutants F63P/F70P and I66P/V73P showed no fusion after 10 min at pH 5 and RT or after an additional 10 min at pH 5 and 37°C, similar to those transfected with V55P/S71P (21) (Fig. 3C). No fusion was seen with the double mutants even if they were left for 30 min at pH 5 and 37°C (unpublished observations). To determine whether the double mutants caused restricted hemifusion, we added 0.5 mM chlorpromazine (CPZ) after exposure to low pH (1). CPZ did not promote fusion for the mutants tested, F63P/F70P and I66P/V73P (unpublished observations).

Conformational changes. Since the two new double mutants, F63P/F70P and I66P/V73P, showed no fusion activity, we analyzed their ability to undergo key conformational changes. We tested for separation of the head groups by monitoring exposure of the epitope for the 12CA5 MAb (30), for exposure of the helix-to-loop region (HA2 106-112) with the LC89 MAb (28), and for exposure of the fusion peptides using an anti-fusion peptide antibody (30). Soluble ectodomains of WT and mutant HA were adjusted to various pH values for 2 min at 37°C, reneutralized, and then immunoprecipitated. All of the mutants analyzed were precipitated with MAb 12CA5 (Fig. 4A), MAb LC89 (Fig. 4B), and the fusion peptide antibody (Fig. 4C) with a pH dependence similar to that for WT HA.

Hydrophobic binding of HA to target membranes. Because the fusion peptides might be exposed but unable to bind to target membranes, we tested F63P/F70P for its ability to bind to liposomes after exposure to low pH using a liposome flotation assay. F63P/F70P HA associated with liposomes as well as WT HA at pH 5 (Fig. 5). Moreover, like that of WT HA, binding of F63P/F70P HA to liposomes was resistant to exposure to 6 M urea or 1 M KI.

We also tested the ability of the full-length, membrane-anchored, F63P/F70P mutant to bind RBCs through the fusion peptide by an NA resistance assay (10). HA initially binds RBCs through an interaction with sialic acid on the surfaces of RBCs. We bound RBCs to NIH 3T3 cells expressing WT and F63P/F70P HA. If these cells were not acidified but were treated with NA to remove sialic acid from the RBCs, most of the RBCs were easily washed away (Fig. 6, first [left] column). Upon acidification, WT HA caused the RBCs to fuse with the HA-expressing cells (Fig. 6, second column), and therefore they could not be removed by NA treatment. The RBCs were not released after NA treatment of low-pH-treated cells expressing F63P/F70P HA (Fig. 6, fourth column). As a control, we verified that this NA treatment removed RBCs from cells expressing the HA0 form of F63P/F70P after low-pH treatment (data not shown).

Coiled-coil formation. Fusion-incompetent mutant F63P/F70P clearly underwent key conformational changes (head group separation, fusion peptide exposure, and exposure of the helix-to-loop region) and clearly bound strongly to target membranes, yet it did not cause fusion. We therefore used several different methods to test whether it forms a complete coiled coil. The F63P and F70P mutations were introduced into recombinant fragment SHA2, which represents residues 33 to 127 of HA2. While this mutant formed trimers (Fig. 7A), presumably through coiled-coil interactions, CD analysis showed reduced α-helicity compared to that for the WT at both pH 7 and 5 (Fig. 7B). We predicted that this mutant would not form a complete and stable coiled coil but rather that the α-helices would be splayed at the N terminus. To test this hypothesis, WT and F63P/F70P SHA2 were treated with thermolysin (1 μg of thermolysin/40-μl reaction volume; conditions corresponding to lanes 3 and 6 in Fig. 7C) and then were subjected to N-terminal sequence analysis. The major sequence for WT SHA2 was LKSTQAAIDQ, which corresponds to the HA2 sequence beginning at residue 38. For F63P/F70P SHA2, the major sequence was IEKEPSEVEG,

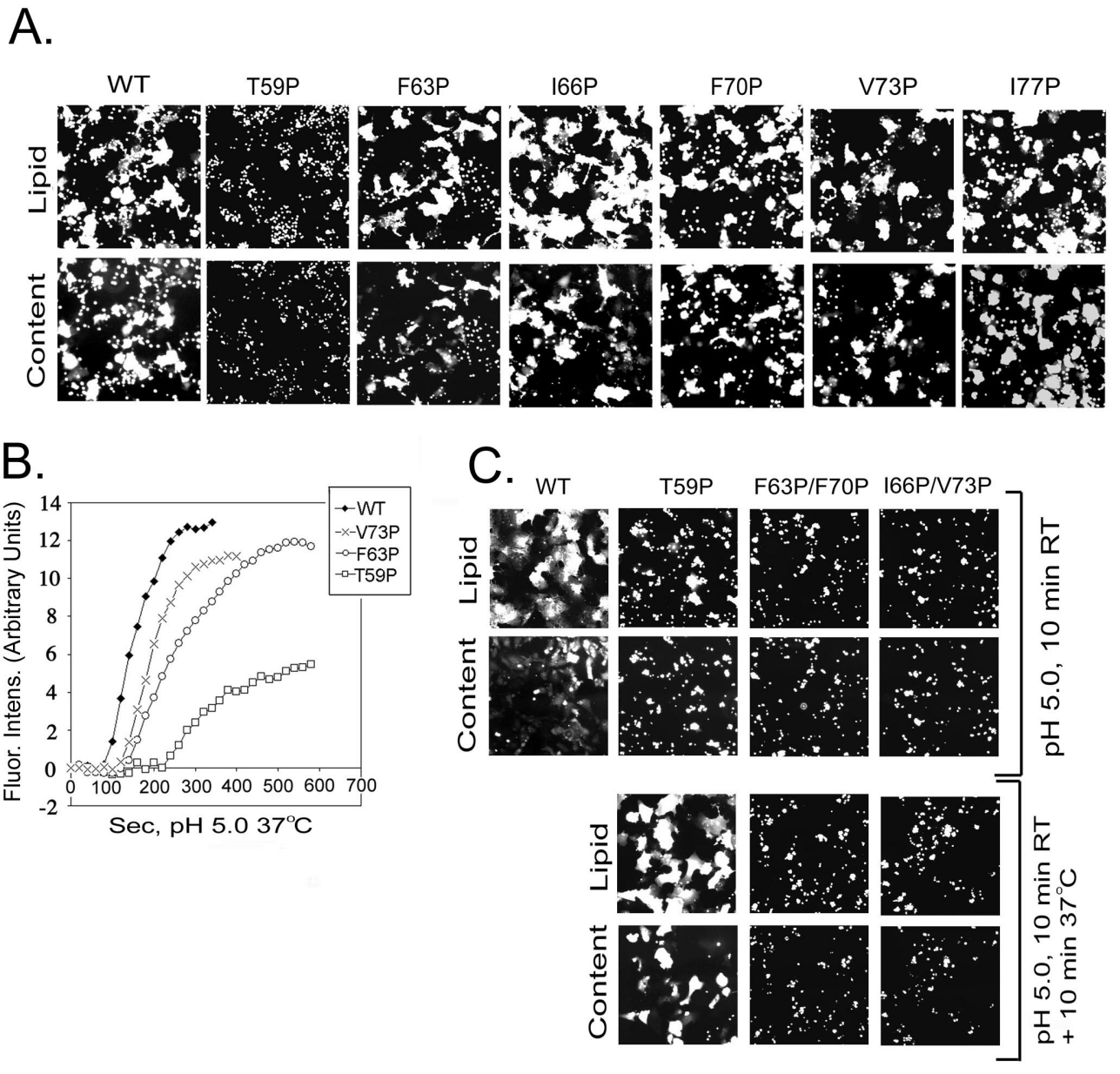

FIG. 3. Fusion. (A) CV-1 cells expressing WT HA or HAs with a single proline substitutions were processed for fusion with RBCs labeled with R18 (lipid probe) and carboxyfluorescein (content probe). Cells were treated with fusion buffer at pH 5.0 for 10 min at RT and then returned to buffer at neutral pH and imaged using fluorescence microscopy. (B) HA-expressing CV-1 cells were processed for the kinetic fusion assay as described in Materials and Methods. (C) HA-expressing cells were processed for fusion as for panel A. The indicated cells (C, bottom) were then returned to pH 5.0 fusion buffer for an additional 10 min at 37°C, reneutralized, and imaged. FACS, performed in parallel, verified that mutant HAs were expressed at equivalent or greater levels than WT HA.

which corresponds to the HA2 sequence beginning at residue 66; a minor sequence VIEKTNEKPH, which corresponds to the HA2 sequence beginning at residue 55, was also observed.

To assess whether the coiled coil of F63P/F70P HA is less stable than that of WT HA in intact HA, the thermolysin sensitivities of the WT and F63P/F70P HA ectodomains were also compared. When low-pH-treated WT and F63P/F70P HA ectodomains were treated with increasing concentrations of thermolysin (Fig. 7D), WT HA2 was resistant to digestion at the highest concentration tested, while 10-fold-less thermolysin was sufficient to digest F63P/F70P HA2. In a complementary experiment (Fig. 7E), a more stringent thermolysin treatment resulted in digestion of WT HA2 at 10 μg of thermolysin/30-μl reaction volume. F63P/F70P HA2 was digested with 100-fold-less thermolysin. Fusion-competent mutant F63P showed, however, the same sensitivity to thermolysin digestion as WT HA2. The faint bands seen in Fig. 7E, right lane, for WT and F63P HA2 are approximately the size of that for TBHA2, the stable core of HA2. A truncated form of F63P/F70P would not have appeared on these gels (Fig. 7E legend provides details). Together, these data suggest that the fusion-active F63P HA, like WT HA, is able to form a complete coiled coil, while the

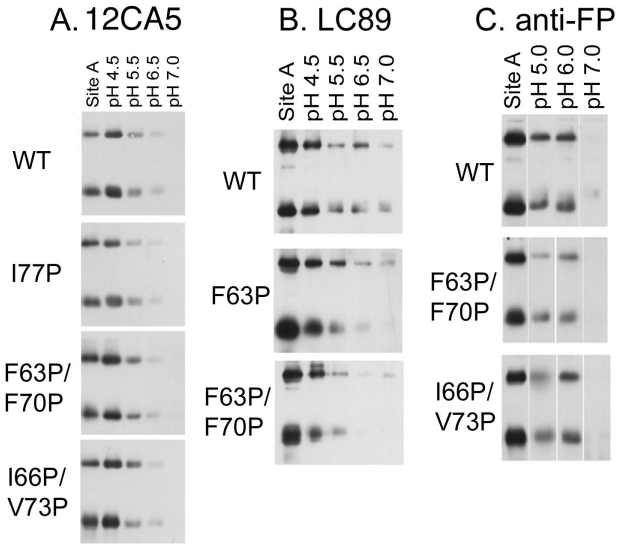

FIG. 4. Conformational changes. GPI-HA-expressing CV-1 cells were processed for conformational-change assays with the indicated antibody as described in Materials and Methods. The 12CA5 epitope is in the interface between the HA1 head groups, the LC89 epitope is the helix-to-loop region of HA2 (residues 106 to 113) (28), and the anti-FP epitope is the HA fusion peptide. The Site A MAb, which is not conformation specific, was used as a control.

fusion-incompetent F63P/F70P HA forms an incomplete coiled coil that is disrupted at its N terminus, primarily above residue 66 (Fig. 1C).

If F63P/F70P HA does not form a complete coiled coil, the fusion peptides of the trimer are not in close contact with each other, and therefore this mutant may not be able to form rosettes, aggregates of HA trimers formed through hydrophobic interactions of the N-terminal fusion peptides. F63P/F70P

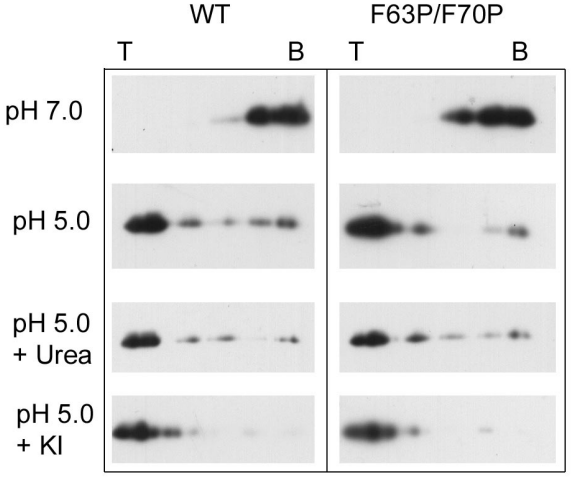

FIG. 5. Liposome binding. GPI-HA-expressing CV-1 cells were treated with trypsin and then with PIPLC to release HA ectodomains. Released material was mixed with liposomes and acidified as described in Materials and Methods. Following reneutralization, samples were mixed with sucrose alone or, where indicated, with sucrose plus urea or KI to form the bottom fraction of a step sucrose gradient. After centrifugation, gradients were fractionated and analyzed by SDS-PAGE as for Fig. 1. T, top; B, bottom.

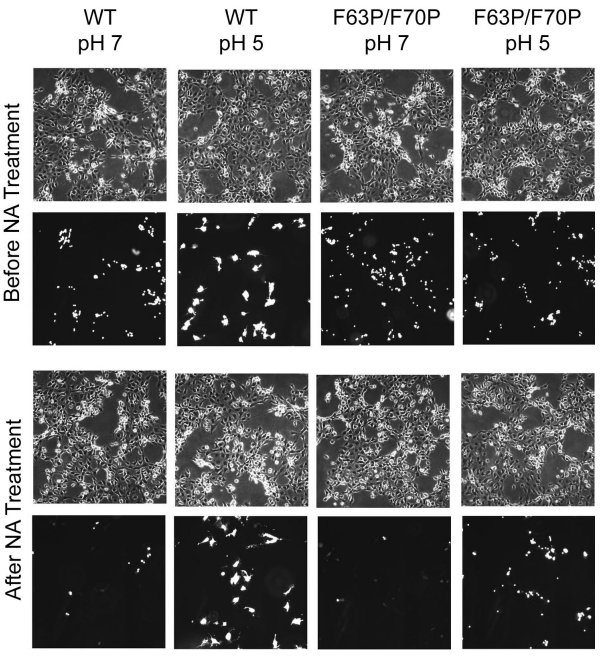

FIG. 6. NA-resistant RBC binding. HA-expressing NIH 3T3 cells were prepared and acidified as for fusion experiments. Phase (first [top] row) and fluorescence (second row) images of bound RBCs were collected. The cells were treated with NA and then washed to remove loosely adhered RBCs. Cells were imaged again using phase (third row) and fluorescence (fourth row) microscopy.

and F63P (which causes fusion like WT HA) were tested for the ability to form rosettes. At pH 7, F63P HA ran in the middle of the gradient (Fig. 8A), similar to WT HA (unpublished observations). After low-pH treatment, F63P HA ran at a lower position, similar to low-pH-treated WT HA (Fig. 8A). In contrast, after exposure to low pH, F63P/F70P HA ran at the position of the original trimer, rather than as an aggregate. EM was also used to examine WT and F63P/F70P HA ectodomains after acidification. WT HA formed rosettes, while F63P/F70P did not (Fig. 8B and C).

If the coiled coil of F63P/F70P is splayed at its N terminus, a further prediction is that, after liposome binding, the spikes of F63P/F70P will be much shorter than those of WT HA. Based on the crystal structure of HA2 and our sequence analysis of thermolysin-digested F73P/F70P, the F63P/F70P HA spikes were predicted to be ~55 Å, about one-half the length of WT spikes. To test this, purified F63P/F70P and WT HA ectodomains were mixed with liposomes and the mixtures were exposed to low pH and examined by EM. WT HA formed spikes that were measured to be 82.0 ± 22.5 Å, while F63P/F70P HA bound to liposomes as short spikes that were measured to be 48.9 ± 14.9 Å (Fig. 9A and B) A diagrammatic representation of how WT HA and F63P/F70P HA could bind to liposomes is shown in Fig. 9C. The observed length of the F63P/F70P spike, coupled with the fact that it is recognized by the LC89 antibody (Fig. 4B), suggests that the helix-to-loop change (Fig. 1, purple) has occurred in this fusion-incompetent mutant (Fig. 1C and 9C).

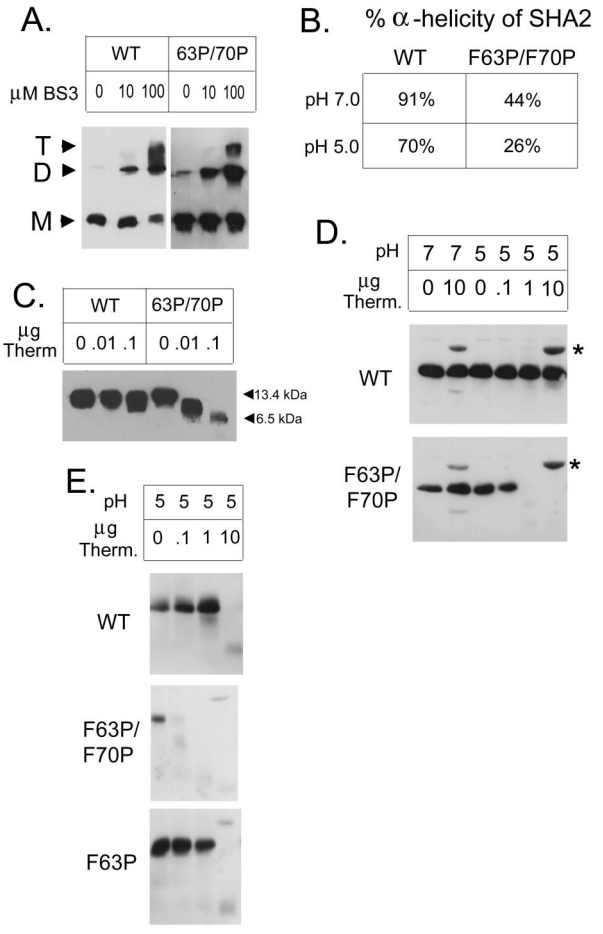

FIG. 7. Characterization of HA2 coiled coils. (A) WT and F63P/F70P SHA2 were treated with 0, 10, or 100 μM BS3 for 30 min at RT. Samples were then boiled and analyzed as for Fig. 2A, with the exception that the SHA2 antibody was used to probe the blots. Arrowheads, monomer (M), dimer (D), and trimer (T) bands. (B) Percent α-helicities of WT and F63P/F70P SHA2 were determined as described in Materials and Methods. (C) WT and F63P/F70P SHA2 were treated with the indicated amounts of thermolysin (in a volume of 10 μl) for 30 min at 37°C. Samples were boiled and analyzed as for panel A, except that the samples were run on a 15% gel rather than a 12% gel. (D) CV-1 cells expressing WT or mutant GPI-anchored HAs were treated with trypsin and then with PIPLC. Released material was acidified to pH 5 for 10 min at RT and then treated with the indicated amounts of thermolysin (in a volume of 30 μl) for 1 h at RT. Samples were run on a 12% gel and analyzed with the SHA2 antibody as for panel A. The major bands represent WT and F63P/F70P HA2 (~27 kDa). At the highest concentration of thermolysin, a band at the molecular mass of thermolysin was seen (34 kDa; *). (E) Samples of HA ectodomains were prepared as for panel D, with the exceptions that the acidification was for 2 min at 37°C and the samples were incubated overnight at 4°C. Samples were run on a 12% gel and analyzed as for panel D. The faint bands seen in the right lanes for WT and F63P HA2 are approximately 22 kDa and therefore likely represent a fragment similar to TBHA2. As in panel D, the major bands represent HA2 (~27 kDa).

DISCUSSION

We previously suggested, based on two proline mutants (V55P and V55P/S71P), that the spring-loaded conformational change of influenza virus HA, the B loop-to-helix transition, is required for fusion (21). We did not, however, uncover the basis for the fusion defect of either mutant, and the role of the spring-loaded conformational change has remained controversial (5, 13, 25). We have now made a complete set of eight proline substitutions at all "a" and "d" positions of the B region of the final coiled coil (Fig. 1A and B). Among mutants with these substitutions, V55P and T59P are impaired for fusion and all three double-proline-substitution mutants that are expressed at the cell surface (V55P/S71P, F63P/F70P, and I66P/V73P) display no fusion activity, either lipid or content mixing. A thorough biochemical analysis of F63P/F70P revealed that it undergoes key low-pH-induced conformational changes including fusion peptide exposure and hydrophobic binding to target membranes.

Several lines of evidence, including N-terminal sequence analysis and EM observations, indicate that F63P/F70P does not form a coiled coil in the N-terminal half of its HA2 subunit. These observations coupled with the fact that prolines in "a" and "d" positions tend to splay helices away from the center of the coiled coil (32) support the notion that the coiled coil of F63P/F70P is splayed in its N-terminal half. Because F63P/F70P does not cause any fusion but is fully competent to bind to target membranes, there must be a role for the complete coiled coil, especially its N-terminal half, beyond simply presenting the fusion peptides to the target membrane. Our current working model is that tension created by binding the C-terminal extended regions into the grooves between the helices of the N-terminal half of the

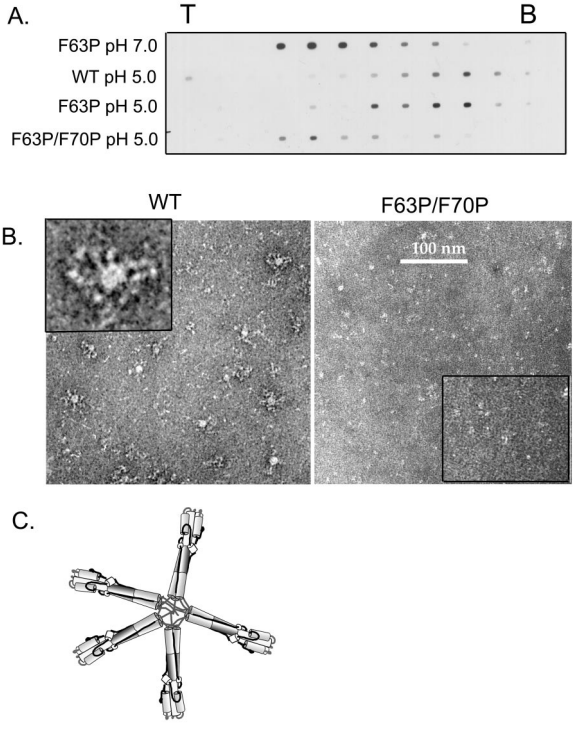

FIG. 8. Rosette formation. (A) PIPLC-released WT and mutant HAs, which were purified as described in Materials and Methods, were acidified, reneutralized, and run on a sucrose gradient. T, top fraction; B, bottom fraction. (B) EM images of proteins prepared essentially as described for panel A prior to application to sucrose gradients. The 100-nm bar applies to both images. Insets are enlarged 3.6-fold. (C) Model for the structure of rosettes formed from WT HA ectodomains.

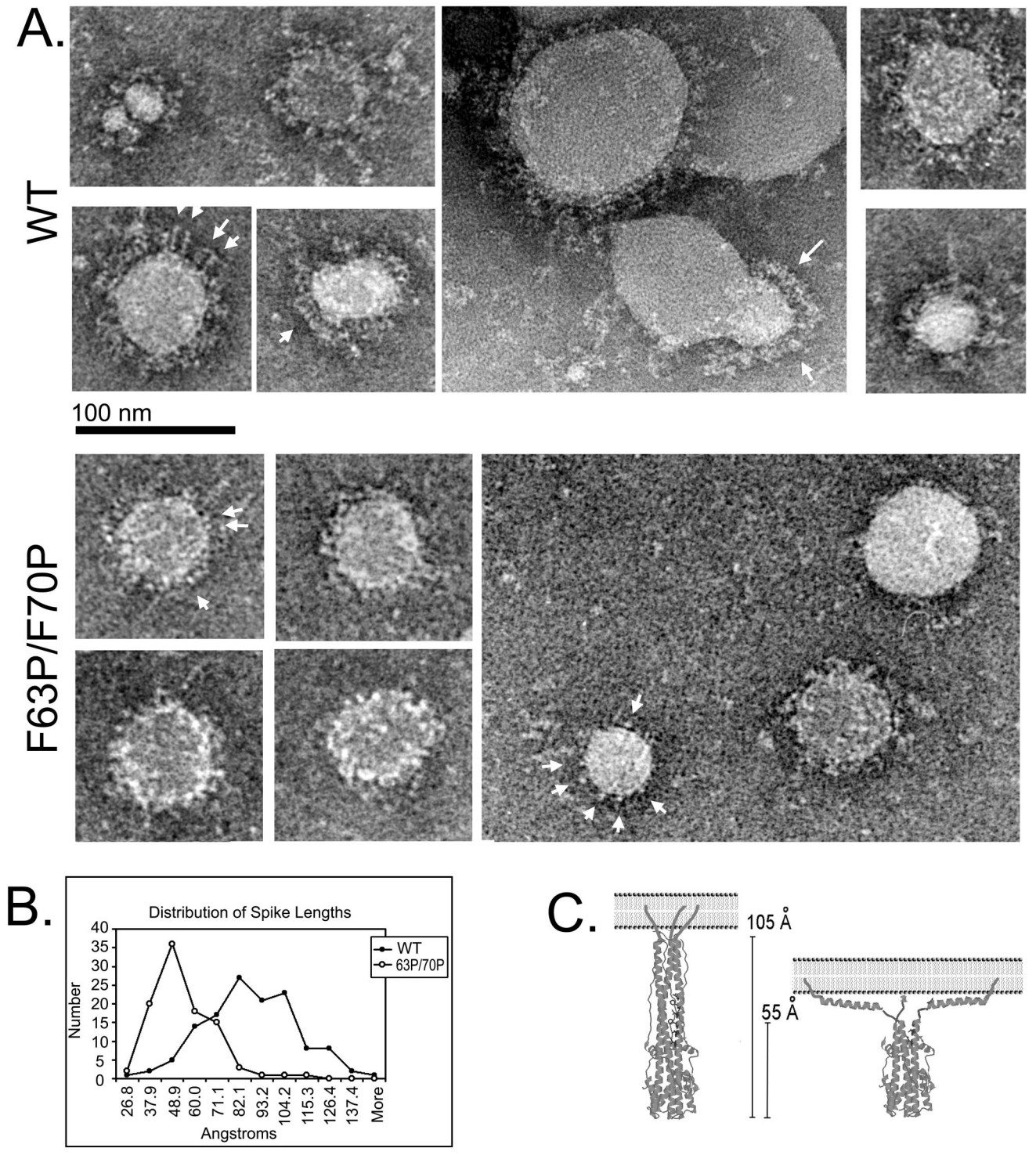

FIG. 9. EM. (A) Purified WT and F63P/F70P HA ectodomains were mixed with liposomes, acidified, reneutralized, and then imaged by low-dose EM. Arrows, proteins on the surfaces of the liposomes. (B) Distribution of HA spike lengths, measured in Photoshop from scanned images. (C) Model for binding of WT and F63P/F70P mutant HA to lipid bilayer.

coiled coil drives fusion. The disruption of the membrane-proximal region of the six-stranded bundle that occurs in the case of F63P/F70P would then prevent fusion but not target membrane binding because it is unable to provide the needed tension. Other non-mutually exclusive possibilities are that the mutations prevent the fusion peptides from one trimer from coming into close proximity and that they prevent higher-order clustering of HA trimers at the fusion site (4, 11).

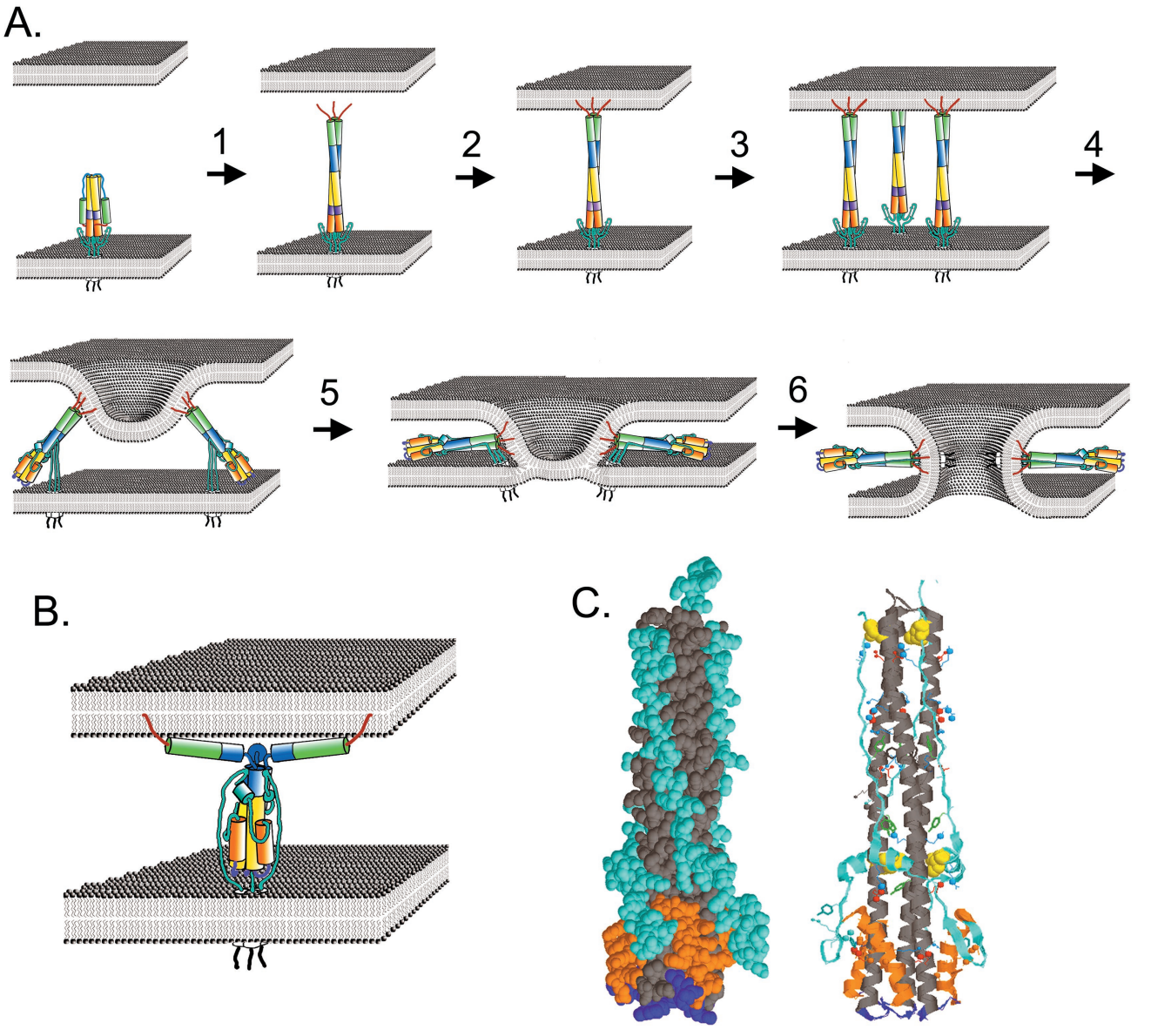

FIG. 10. Model for HA-mediated fusion and fusion blocked by mutant HA. (A) Fusion model. HA1 is omitted for clarity. The model is a revised version of that from references 14 and 29; steps 1 to 3 are as described in these references. The kink region (purple) refolds from a helix to a loop, and the D helix (orange) reverses direction to lie antiparallel to the coiled coil. The extended C termini of HA2 bind in the grooves between the helices of the coiled coil, causing the trimer to tilt and the membranes to merge (steps 4 and 5). The fusion peptides and transmembrane domains are brought together, breaking the hemifusion diaphragm (step 6). (B) Model of F63P/F70P HA. (C) Interactions between the coiled coil and the extended C-terminal region. (Left) Space-filling model of the EHA2 crystal structure. Gray, coiled-coil region (HA2 33-105); purple, helix-to-loop region (HA2 106-111); orange, D helix region (HA2 112-129); light blue, C-terminal region (HA2 130-185). (Right) Ribbon diagram, colored as for the left image, except as noted below, showing potential noncovalent interactions between the coiled coil and the rest of the EHA2 structure. Residue colors are as follows: basic residues, blue; acidic residues, red; tyrosines involved in cation-pi interactions, green; hydrophobic residues, yellow. Salt bridges and cation-pi interactions were predicted from the protein database file 1QU1 by the program Protein Explorer, and interactions not involved in contacts between the coiled coil and residues 112 to 185 are shown in the same color as the region in which they are found.

Implications for models of HA-mediated fusion. For viral fusion proteins, fusion could be driven by destabilization of the membranes by the fusion peptide, by energy released by the spring-loaded conformational change or other conformational changes, or by some combination of the two. Models for HA-mediated fusion that do not require the spring-loaded conformational change but rather rely primarily on the fusion peptide have been proposed (3, 5, 26). Our findings, however, argue strongly that binding of the fusion peptides to the target membrane is not sufficient. Fusion-incompetent mutant F63P/F70P protrudes ~55 Å from the surfaces of liposomes (Fig. 9), suggesting that during aborted fusion it could bring two membranes within 55 Å of each other (Fig. 10B). The approximate width of native HA at the level of the fusion peptides is 55 Å,

which is, therefore, the distance between the membranes immediately before fusion predicted by the model in reference 26. The lack of lipid mixing with F63P/F70P, even after long periods of low-pH incubation, indicates that even hemifusion (Fig. 10A, step 5) requires more than simple proximity of the membranes in the presence of bound fusion peptides

Our results with F63P/F70P support models in which conformational changes in HA drive fusion. In one group of HA fusion models which invoke the spring-loaded conformational change, this change, the B loop-to-helix transition, is proposed to be the major driving force for mediating the lipid mixing stage of fusion (2, 17). However, in our model 14, 29; see also the White laboratory website) (Fig. 10 shows the revised version), the spring-loaded conformational change is required, but is not sufficient, for fusion. We propose that binding the C terminus of the HA2 ectodomain (residues 113 to 175; orange and light blue in Fig. 1 and 10) to the grooves of the N-terminal coiled coil creates the tension needed to pull the membranes together. Transition to the final low-pH form would then provide the energy for the first stage of fusion, outer leaflet lipid mixing (Fig. 10A, step 5). Antiparallel packing of the D helix (orange in Fig. 1 and 10) against the coiled coil is likely not sufficient to drive lipid mixing, since these interactions probably occur in F63P/F70P (Fig. 9 and 10B; see also Results). We further propose that transition from hemifusion to the fusion pore (Fig. 10A, step 6) depends, in part, on subsequent action of the fusion peptide (20) and the transmembrane domain (1) on the hemifusion diaphragm (Fig. 10A, step 6).

An examination of interactions between the coiled coil and the C-terminal end of the HA2 ectodomain (residues 113 to 175) reveals five salt bridges and three cation-pi interactions per monomer of HA (Fig. 10C). Given an estimate of −5 kcal/mol per salt bridge (24), the energy to form 15 salt bridges (in one trimer) is −75 kcal/mol, similar to the estimated energy of formation of the coiled coil (−30 to −60 kcal/mol) (2). Additional sources of energy could come from other types of interactions along the outside surface of the coiled coil (e.g., the cation-pi interactions, hydrogen bonding, and hydrophobic interactions [9]).

Relation to other coiled-coil viral fusion proteins. The possibility that the inability of F63P/F70P to form a tight six-stranded bundle in its membrane-proximal region leads to loss of tension to drive fusion has analogies with results for other viral fusion proteins that employ coiled coils and six-helix bundle formation. It has been shown for human immunodeficiency virus type 1 (HIV-1) Env and simian virus 5 (SV5) F that the six-helix bundle is necessary for fusion (19, 22). For HIV-1 Env, the transition to this bundle, not just its presence, is believed to provide the energy to drive fusion. For HA, only a small portion of the C-terminal region, which binds to the coiled coil, is helical; the rest is extended in an approximately polyproline type II conformation (9) and binds in the groove between the helices of the coiled coil. The combination of this extended region and the short helical region may therefore be functionally equivalent to the C-terminal helix of HIV-1 Env, which also binds in the groove between the helices of the coiled coil (27). The homologous C-terminal region of the SV5 F protein is also largely helical, although the membrane-proximal segment is missing from the structure, and therefore is of unknown structure. Other viral coiled-coil fusion proteins contain a combination of extended and helical structures in their C-terminal regions. Human T-cell leukemia virus type 1 gp21, for example, is primarily extended in this region and contains only a short helical section. Despite their morphological variety, the C-terminal regions of the ectodomains of all of these different fusion proteins may serve the same function: to bind to the coiled coil and thereby provide tension to drive fusion.

ACKNOWLEDGMENTS

We thank Samuel Green and David Castle for critical reading of the manuscript, Leonid Chernomordik and Yeon-Kyun Shin for reagents, and the University of Virginia DNA sequencing, protein sequencing, and FACS facilities.

The work was supported by a grant from the NIH (AI22470) to J. White and by grants from the NIH (AI41644) and NSF (MCB-9904879) to J. Brown. J. Gruenke was supported in part by the Cell and Molecular Biology Training Program (University of Virginia).

REFERENCES

1. **Armstrong, R. T., A. Kushnir, and J. M. White.** 2000. The transmembrane domain of influenza virus hemagglutinin exhibits a stringent length requirement to promote the hemifusion to fusion transition. J. Cell Biol. **151:**425–438.
2. **Bentz, J.** 2000. Membrane fusion mediated by coiled coils: a hypothesis. Biophys. J. **78:**886–900.
3. **Bentz, J., H. Ellens, and D. Alford.** 1990. An architecture for the fusion site of influenza hemagglutinin. FEBS Lett. **276:**1–5.
4. **Blumenthal, R., D. P. Sarkar, S. Durell, D. E. Howard, and S. J. Morris.** 1996. Dilation of the influenza hemagglutinin fusion pore revealed by kinetics of individual cell-cell fusion events. J. Cell Biol. **135:**63–71.
5. **Bonnafous, P., and T. Stegmann.** 2000. Membrane perturbation and fusion pore formation in influenza hemagglutinin-mediated membrane fusion: a new model for fusion. J. Biol. Chem. **275:**6160–6166.
6. **Bullough, P. A., F. M. Hughson, J. J. Skehel, and D. C. Wiley.** 1994. Structure of influenza haemagglutinin at the pH of membrane fusion. Nature **371:**37–43.
7. **Carr, C. M., and P. S. Kim.** 1993. A spring-loaded mechanism for the conformational change of influenza hemagglutinin. Cell **73:**823–832.
8. **Chen, J., K. H. Lee, D. A. Steinhauer, D. J. Stevens, J. J. Skehel, and D. C. Wiley.** 1998. Structure of the hemagglutinin precursor cleavage site, a determinant of influenza pathogenicity and the origin of the labile conformation. Cell **95:**409–417.
9. **Chen, J., J. J. Skehel, and D. C. Wiley.** 1999. N- and C-terminal residues combine in the fusion-pH influenza hemagglutinin HA(2) subunit to form an N cap that terminates the triple-stranded coiled coil. Proc. Natl. Acad. Sci. USA **96:**8967–8972.
10. **Chernomordik, L. V., V. A. Frolov, E. Leikina, P. Bronk, and J. Zimmerberg.** 1998. The pathway of membrane fusion catalyzed by influenza hemagglutinin: restriction of lipids, hemifusion, and lipidic pore formation. J. Cell Biol. **140:**1369–1382.
11. **Danieli, T., S. L. Pelletier, Y. I. Henis, and J. M. White.** 1996. Membrane fusion mediated by the influenza virus hemagglutinin requires the concerted action of at least three hemagglutinin trimers. J. Cell Biol. **133:**559–569.
12. **Delos, S. E., J. M. Gilbert, and J. M. White.** 2000. The central proline of an internal viral fusion peptide serves two important roles. J. Virol. **74:**1686–1693.
13. **Epand, R. F., J. C. Macosko, C. J. Russell, Y. Shin, and R. M. Epand.** 1999. The ectodomain of HA2 of influenza virus promotes rapid pH dependent membrane fusion. J. Mol. Biol. **286:**489–503.
14. **Hernandez, L. D., L. R. Hoffman, T. G. Wolfsberg, and J. M. White.** 1996. Virus-cell and cell-cell fusion. Annu. Rev. Cell Dev. Biol. **12:**627–661.
15. **Hernandez, L. D., R. R. Peters, S. E. Delos, Y. A. T. Young, D. A. Agard, and J. M. White.** 1997. Activation of a retroviral membrane fusion protein: soluble receptor induced liposome binding of the ALSV envelope glycoprotein. J. Cell Biol. **139:**1455–1464.
16. **Koke, J. A., M. Yang, D. J. Henner, J. J. Volwerk, and O. H. Griffith.** 1991. High-level expression in Escherichia coli and rapid purification of phosphatidylinositol-specific phospholipase C from Bacillus cereus and Bacillus thuringiensis. Protein Expr. Purif. **2:**51–58.
17. **Kozlov, M. M., and L. V. Chernomordik.** 1998. A mechanism of protein-mediated fusion: coupling between refolding of the influenza hemagglutinin and rearrangements. Biophys. J. **75:**1384–1396.
18. **Melikyan, G. B., S. Lin, M. G. Roth, and F. S. Cohen.** 1999. Amino acid sequence requirements of the transmembrane and cytoplasmic domains of influenza virus hemagglutinin for viable membrane fusion. Mol. Biol. Cell **10:**1821–1836.
19. **Melikyan, G. B., R. M. Markosyan, H. Hemmati, M. K. Delmedico, D. M.**

Lambert, and F. S. Cohen. 2000. Evidence that the transition of HIV-1 gp41 into a six-helix bundle, not the bundle configuration, induces membrane fusion. J. Cell Biol. **151:**413–423.

20. **Qiao, H., T. Armstrong, G. B. Melikyan, F. S. Cohen, and J. M. White.** 1999. A specific point mutation at position 1 of the influenza hemagglutinin fusion peptide displays a hemifusion phenotype. Mol. Biol. Cell **10:**2759–2769.
21. **Qiao, H., S. Pelletier, L. Hoffman, J. Hacker, R. T. Armstrong, and J. M. White.** 1998. Specific single or double proline substitutions in the "spring-loaded" coiled-coil region of the influenza hemagglutinin impair or abolish membrane fusion activity. J. Cell Biol. **141:**1335–1347.
22. **Russell, C. J., T. S. Jardetzky, and R. A. Lamb.** 2001. Membrane fusion machines of paramyxoviruses: capture of intermediates of fusion. EMBO J. **20:**4024–4034.
23. **Sayle, R. A., and E. J. Milner-White.** 1995. RASMOL: biomolecular graphics for all. Trends Biochem. Sci. **20:**374.
24. **Schulz, G. E., and R. H. Schirmer.** 1979. Principles of protein structure, 2nd ed. Springer-Verlag, New York, N.Y.
25. **Shangguan, T., D. P. Siegel, J. D. Lear, P. H. Axelsen, D. Alford, and J. Bentz.** 1998. Morphological changes and fusogenic activity of influenza virus hemagglutinin. Biophys. J. **74:**54–62.
26. **Stegmann, T., J. M. White, and A. Helenius.** 1990. Intermediates in influenza-induced membrane fusion. EMBO J. **9:**4231–4241.
27. **Weissenhorn, W., A. Dessen, S. C. Harrison, J. J. Skehel, and D. C. Wiley.** 1997. Atomic structure of the ectodomain from HIV-1 gp41. Nature **387:**426–430.
28. **Wharton, S. A., L. J. Calder, R. W. H. Ruigrok, J. J. Skehel, D. A. Steinhauer, and D. C. Wiley.** 1995. Electron microscopy of antibody complexes of influenza virus haemagglutinin in the fusion pH conformation. EMBO J. **14:**240–246.
29. **White, J. M.** 1995. Membrane fusion: the influenza paradigm. Cold Spring Harbor Symp. Quant. Biol. **60:**581–588.
30. **White, J. M., and I. A. Wilson.** 1987. Anti-peptide antibodies detect steps in a protein conformational change: low-pH activation of the influenza virus hemagglutinin. J. Cell Biol. **105:**2887–2896.
31. **Wilson, I. A., J. J. Skehel, and D. C. Wiley.** 1981. Structure of the haemagglutinin membrane glycoprotein of influenza virus at 3 Å resolution. Nature **289:**366–372.
32. **Woolfson, D. N., and D. H. Williams.** 1990. The influence of proline residues on alpha-helical structure. FEBS Lett. **277:**185–188.
33. **You, J., M. Kamihira, and S. Iijima.** 1999. Enhancement of transfection efficiency by protamine in DDAB lipid vesicle-mediated gene transfer. J. Biochem. (Tokyo) **125:**1160–1167.